Available online at www.sciencedirect.com
ScienceDirect
Trans. Nonferrous Met. Soc. China 35(2025) 3520−3532
Transactions of Nonferrous Metals Society of China
www.tnmsc.cn

Regeneration of battery grade $FePO_4$ and Li_2CO_3 from Al/F-bearing spent $LiFePO_4$/C powder

Ye-hui-zi WU, Kang-gen ZHOU, Chang-hong PENG, Kui YI, Jing-kun DENG, Zai-rong QIU, Wei CHEN, Ke-jing ZHANG

School of Metallurgy and Environment, Central South University, Changsha 410083, China

Received 3 January 2024; accepted 27 May 2024

Abstract: A sustainable approach for recovering battery grade $FePO_4$ and Li_2CO_3 from Al/F-bearing spent $LiFePO_4$/C powder was proposed, including acid leaching, fluorinated coordination precipitation, homogeneous precipitation, and high-temperature precipitation. Under the optimal conditions, the leaching efficiencies of Li, Fe, P, Al, and F were 97.6%, 97.1%, 97.1%, 72.5%, and 63.3%, respectively. The effects of different parameters on the removal of Al/F impurities were systematically evaluated, indicating about 99.4% Al and 96.4% F in the leachate were precipitated in the form of $Na_3Li_3Al_2F_{12}$, and their residual concentrations were only 0.0124 and 0.328 g/L, respectively, which could be directly used to prepare battery grade $FePO_4$ (99.68% in purity). Lithium in the Al/F-bearing residue could be extracted through $CaCO_3$−$CaSO_4$ roasting followed by acid leaching, ultimately obtaining 99.87% purity of Li_2CO_3. The recovery rates of Li and Fe were 96.88% and 92.85%, respectively. An economic evaluation demonstrated that the process was profitable.

Key words: Al/F-bearing spent $LiFePO_4$/C powder; sulfuric acid leaching; impurities removal; battery grade iron phosphate; battery grade lithium carbonate

1 Introduction

In light of the strategic objectives of achieving carbon peaking by 2030 and carbon neutrality by 2060 [1], the widespread utilization of $LiFePO_4$ batteries (LFPs) with high energy density and environmental benignity has been significantly advanced in the fields of electric vehicles and energy storage [2]. It is reported that the projected number of electric vehicles on the global scale is expected to reach 145 million by 2030 [3], and the energy storage development will exceed 1095 GW by 2040 [4]. Currently, LFPs are successfully used in Tesla's model 3, BYD's Han EV, and other electric vehicles [5]. However, given the limited life cycle of lithium batteries of 3−5 years [6], about 780000 t of spent lithium batteries are likely to be generated by 2025, and China will hold 400000 t of spent LFPs [7−9].

For the recovery of spent LFPs, traditional direct regeneration methods based on defect-targeted repair involve restoring the electrochemical properties by subjecting them to thermal treatment with additional lithium sources at 600−800 °C [10,11]. Nevertheless, electrochemical performance of regenerated $LiFePO_4$ is always unsatisfactory, owing to the presence of high contents of impurities and great differences in their degree of damage [12]. In comparison, the hydrometallurgical process, including pretreatment, leaching, purification, and product preparation, can effectively address the

Corresponding author: Wei CHEN, Tel: +86-15874966820, E-mail: dvchen@csu.edu.cn;
Ke-jing ZHANG, Tel: +86-13874831786, E-mail: 22022126@csu.edu.cn
https://doi.org/10.1016/S1003-6326(25)66897-X

aforementioned drawbacks [13,14]. Due to the non-selectivity of the acid leaching stage, F and Al impurities originated from the fluorinated electrolyte and current collector Al foil entered the leachate. The ecosystem would be contaminated by F-containing wastewater without appropriate disposals, further causing severe threats to human-beings through the accumulation of the food chain [15]. Moreover, Al impurity would enter the final $FePO_4$ products, ascribing to the similar solubility product between $AlPO_4$ (K_{sp}=9.84×10^{-21}) and $FePO_4·2H_2O$ (K_{sp}=1.3×10^{-22}) [16] and the formation of aluminum-doped solid solutions ($Fe_{1-x}Al_xPO_4$) [17−19], thus adversely affecting the electrochemical performance of regenerated LFPs if the content of Al exceeds 0.05 wt.% [20].

Generally, F is typically removed in the form of HF gas through a high-temperature calcination pretreatment process [21], while the corrosive gas poses serious damage to equipment [22]. Additionally, though the conventional $Al(OH)_3$ precipitation process is cheap and simple to operate, the pH value for Al precipitation is about 3.41 according to the solubility product constants of $Al(OH)_3$ (K_{sp}=1.3×10^{-33}) [23], which would easily result in the formation of $LiFePO_4$ precipitates. As a result, studies on the recycling of spent $LiFePO_4$/C powder primarily focus on the recovery of lithium through oxidative leaching in consideration of economic cost and technical feasibility [24−26], while Fe and P are remained as Fe/P residues (Table S1 in Supporting Information (SI)). The premise of Fe/P recovery from Al-bearing $FePO_4$ residue is the reduction of Fe^{3+} to Fe^{2+}, since the separation of Fe^{3+} and Al^{3+} is extremely difficult due to the similar physiochemical properties, thus resulting in the high reagent cost and the extended process flow. In our recent work, a sulfuric acid leaching followed by solvent extraction process was proposed for the removal of Al to overcome its non-selective leaching behavior for valuable components and impurities [27], but its industrial applicability was limited due to pungent odors and non-fluorinated spent $LiFePO_4$/C powder.

Inspired by the low solubility of lithium-containing aluminum electrolyte (i.e., $Na_3Li_3Al_2F_{12}$) and the considerable amounts of Al and F in Al/F-bearing spent $LiFePO_4$ powder [28], the fluorinated coordination precipitation was proposed to selectively remove Al and F impurities, thus promoting the comprehensive recovery of Li/Fe/P from LFPs. Batch experiments were carried out to determine the operating variables for leaching and fluorinated coordination precipitation, and corresponding characterizations were performed to elucidate the mechanisms. The appropriate temperature for the precipitation of $FePO_4·2H_2O$ from low-Al filtrate was evaluated, and the recovery for lithium in the Al/F-bearing residue was also investigated. A preliminary economic analysis was investigated to determine the economic profits. This study provides a forward-looking guidance for Li/Fe/P recovery from Al/F-bearing spent $LiFePO_4$/C powder sustainably and economically.

2 Experimental

2.1 Materials

The Al/F-bearing spent $LiFePO_4$/C powder was obtained from Shenzhen Zhongjin Lingnan Technology Co., Ltd. (Guangdong, China), and its composition (wt.%) was Al 0.86, Cu 0.002, Fe 21.61, P 11.91, Li 2.73, C 29.85, and F 0.89. All the chemical reagents, including H_2SO_4, NaF, $NH_3·H_2O$, NaOH, $Fe_2(SO_4)_3$, $CaSO_4$, $CaCO_3$, Na_2CO_3, H_2O_2 (30 wt.%), and NaH_2PO_4, were of analytical grade and purchased from Macklin Co. Ltd. Deionized water was used throughout the experiments.

2.2 Procedures

The proposed flow sheet of the comprehensive recovery process for Al/F-bearing spent $LiFePO_4$/C powder is presented in Fig. 1. The comprehensive recovery for Al/F-bearing spent $LiFePO_4$/C powder included sulfuric acid leaching, fluorinated coordination precipitation, synthesis of iron phosphate, and the recovery for lithium carbonate. Firstly, the valuable components in the Al/F-bearing spent $LiFePO_4$/C powder were transferred into the solution through sulfuric acid leaching. Then, appropriate amounts of NaF were added into the leachate for the removal of F and Al impurities. Next, the low-Al filtrate can be directly used to prepare battery grade $FePO_4$, and the Al/F-bearing residue can be recovered in the form of Li_2CO_3 through $CaCO_3$−$CaSO_4$ roasting followed by acid leaching. Three parallel tests were conducted and the average value was reported, and error bars were derived based on the values calculated from standard deviation.

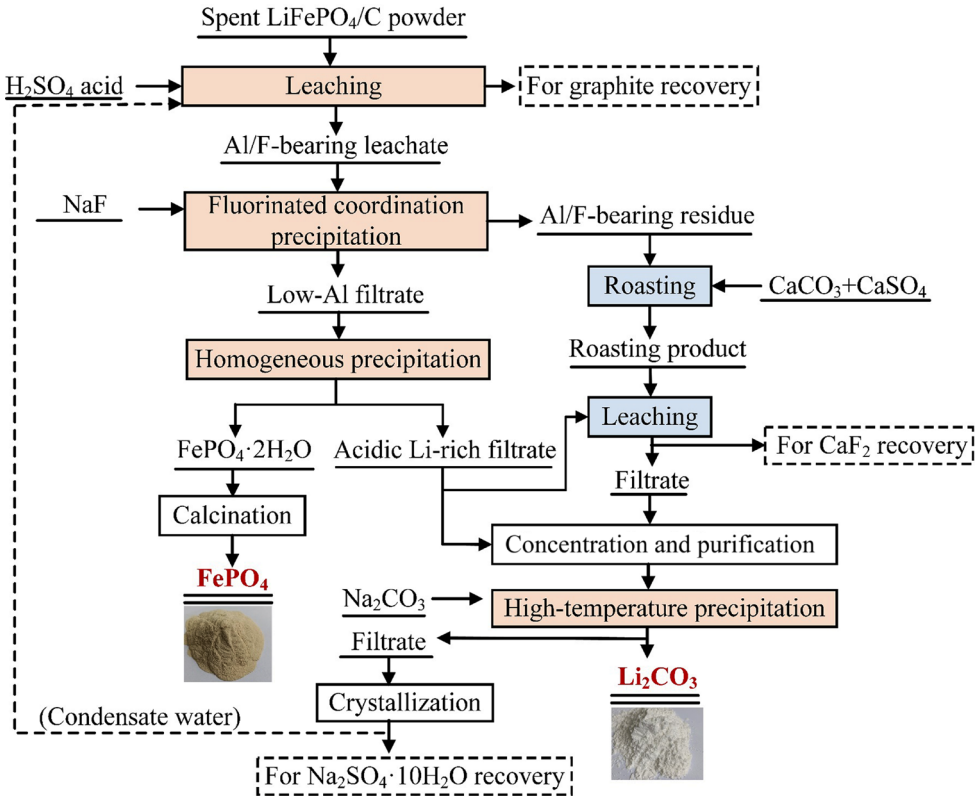

Fig. 1 Schematic illustration of process for regeneration of $FePO_4$ and Li_2CO_3 from Al/F-bearing spent $LiFePO_4$/C powder

The detailed descriptions for each experimental protocol are supplemented in Text S1 of SI.

2.3 Analytical methods

The concentrations of elements were measured by inductively coupled plasma−optical emission spectrometer (ICP−OES, SPECTRO BLUE SOP, Germany). The fluoride concentration was measured by the fluoride-selective electrode (ORION STAR A324, Thermo Fisher Scientific, MA, USA) according to GB 7484—87 Standard. The crystalline phases of the solid were determined by X-ray diffraction with Cu K_α radiation (XRD, PANalytical/Empyrean 2, Netherlands), and the patterns with 2θ ranged from 5° to 90°. The precipitate was also characterized by Fourier transform infrared spectroscopy (FT-IR, NEXUS-Thermo Nicolet Company, USA), X-ray photo-electron spectroscopy (XPS, Thermo Fisher-VG Scientific ESCALAB250Xi, USA), atomic force microscopy (AFM, Bruker Dimension Icon), scanning electron microscopy (SEM, MIRA3 LMH) and energy-dispersive X-ray spectroscopy (EDS, One Max 20).

3 Results and discussion

3.1 Sulfuric acid leaching of Al/F-bearing spent $LiFePO_4$/C powder

The impact of H_2SO_4 concentration on the leaching efficiencies of valuable components was firstly investigated. As shown in Fig. 2(a), the leaching efficiencies of Li, Fe, and P presented a positive correlation with H_2SO_4 concentration, attributing to an enhancement in dissolution of each element under high acidity. As the concentration of H_2SO_4 was 2.1 mol/L, the leaching efficiencies of Al, Li, Fe, and P were 72.5%, 97.6%, 97.1%, and 97.1%, respectively, and the concentration of F was approximately 1878 mg/L. Further increasing H_2SO_4 concentration had negligible impact on the leaching performance of Li/Fe/P, but facilitated the leaching of Al and F impurities. Consequently, the optimal concentration of H_2SO_4 was determined to be 2.1 mol/L, that is, the dosage of H_2SO_4 was 0.5 mol. Additionally, the leaching efficiencies of Li/Fe/P and Al initially increased as the liquid-to-solid ratio increased (Fig. 2(b)), due to the

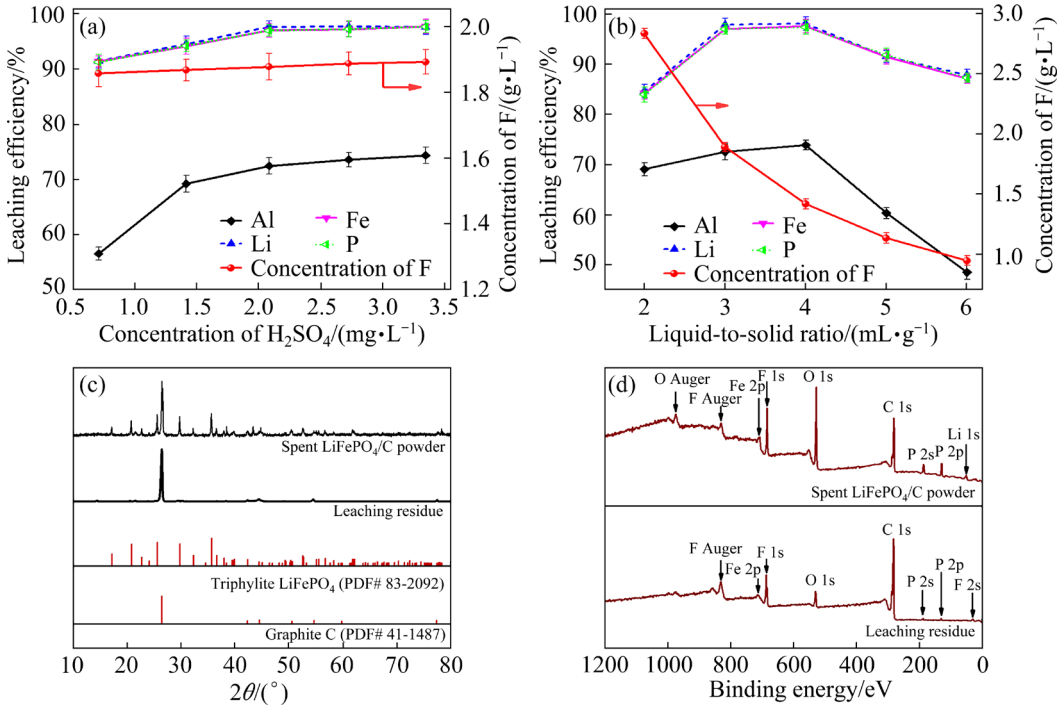

Fig. 2 Effects of (a) concentration of H_2SO_4 (liquid-to-solid ratio of 3 mL/g, 298 K, 120 min) and (b) liquid-to-solid ratio (0.5 mol H_2SO_4, 298 K, 120 min) on leaching efficiency; (c) XRD patterns and (d) XPS spectra of spent $LiFePO_4$/C powder before and after leaching

promotion of the efficient contact area for the solid and liquid phases. However, the leaching efficiencies decreased when the liquid-to-solid ratio exceeded 4 mL/g, because a higher liquid-to-solid ratio resulted in a decrease in acidity. Considering the high viscosity of the slurry at low liquid-to-solid ratios, a liquid-to-solid ratio of 3 mL/g was selected.

Under the optimal conditions of 2.1 mol/L H_2SO_4, liquid-to-solid ratio of 3 mL/g, 298 K, and 120 min, three parallel industrial-scale pilot leaching experiments were conducted using 1000 g Al/F-bearing spent $LiFePO_4$/C powder. The results are presented in Table S2 of SI, and no copper was detected in the leachate. The XRD patterns of the spent $LiFePO_4$/C powder were well-matched with the olivine-structured $LiFePO_4$ (PDF# 83-2092) and graphite (PDF# 41-1489), and only the characteristic peaks of graphite were observed in the leaching residue (Fig. 2(c)). In addition, XPS analyses were performed to identify the chemical composition of the spent $LiFePO_4$/C powder and leaching residue (as presented in Fig. 2(d)). The peaks of Li, Fe, and P almost disappeared in the leaching residue, and the peaks of F and O were drastically reduced. In comparison, the graphite C peak was enhanced in the leaching residue. These findings were consistent with the results presented in Fig. 2(c), indicating that $LiFePO_4$ was almost completely leached.

3.2 Selective fluorinated coordination precipitation for Al/F removal

The leachate generated from sulfuric acid leaching process contains considerable amounts of Al and F impurities, which should be removed prior to the recovery of Li/Fe/P. As shown in Fig. 3(a), the forms of Al−F complexes vary distinctively with the changes of pH value. The thermodynamical feasibility of the reactions for Na_3AlF_6 and Li_3AlF_6 is confirmed by the Gibbs free energies ΔG^{Θ} (Table S3 in SI), implying that the formation of $Na_3Li_3Al_2F_{12}$ composite can occur spontaneously. Consequently, NaF was selected as the precipitant to provide sufficient amounts of Na and F, thus achieving the removal of Al and F in the form of $Na_3Li_3Al_2F_{12}$ from the leachate. As depicted in Fig. 3(b) [29], Li^+, Fe^{2+} and PO_4^{3-} in the solution could be precipitated as $LiFePO_4$ at high pH value. Therefore, the effects of initial pH, precipitant dosage, reaction temperature, and reaction time on the removal of Al/F impurities from the leachate

and the loss of Fe/P/Li were systematically evaluated.

Figure 4(a) shows a remarkable influence of initial pH on the precipitation. The precipitation efficiency of Al reached 98.6% at an initial pH value of 2.1, and remained relatively stable thereafter. The precipitation efficiencies of Fe, Li, and P sharply increased from 1.3%, 9.1%, and 0.9% to 18.6%, 28.6%, and 17.7%, respectively, as the pH value varied from 2.70 to 3.05, indicating a higher pH aggravated the loss of lithium. This can be attributed to the formation of $LiFePO_4$, as evidenced in the XRD pattern of the Al/F-bearing precipitate obtained at pH 3.05 (Fig. S1 in SI). Therefore, considering the tradeoff between the precipitation efficiency of Al and the loss of Li, the optimal initial pH value was adjusted to be 2.4.

Figure 4(b) presents the precipitation performance of Al under varying dosages of NaF precipitant. As the dosage of NaF increased from 0 to 4.2 g, the precipitation efficiency of Al increased from 17.6% to 99.4%, indicating the promotion for the removal of Al with the addition of NaF. Apparently, fluorinated coordination precipitation

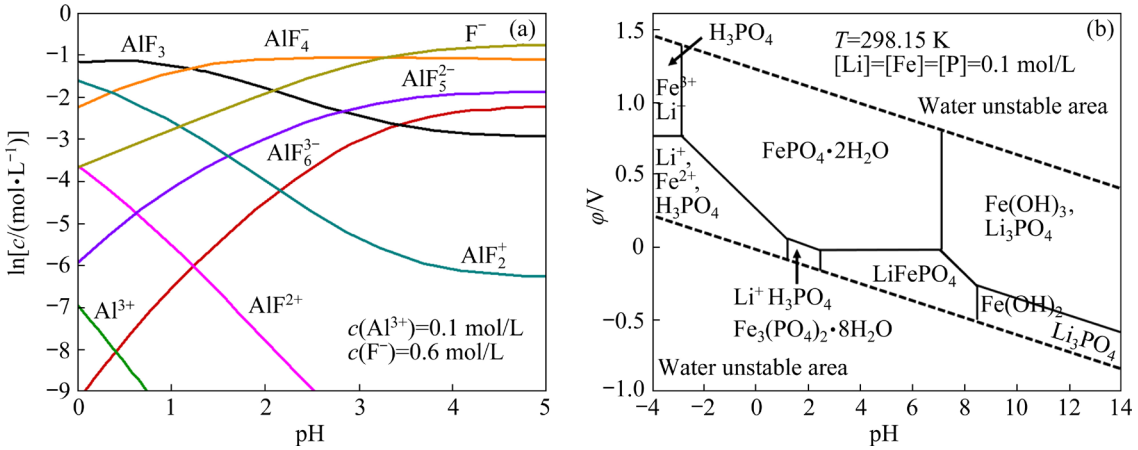

Fig. 3 (a) Different forms of Al–F complexes with changes in pH; (b) φ–pH diagrams for Li–Fe–P–H_2O system at 298.15 K

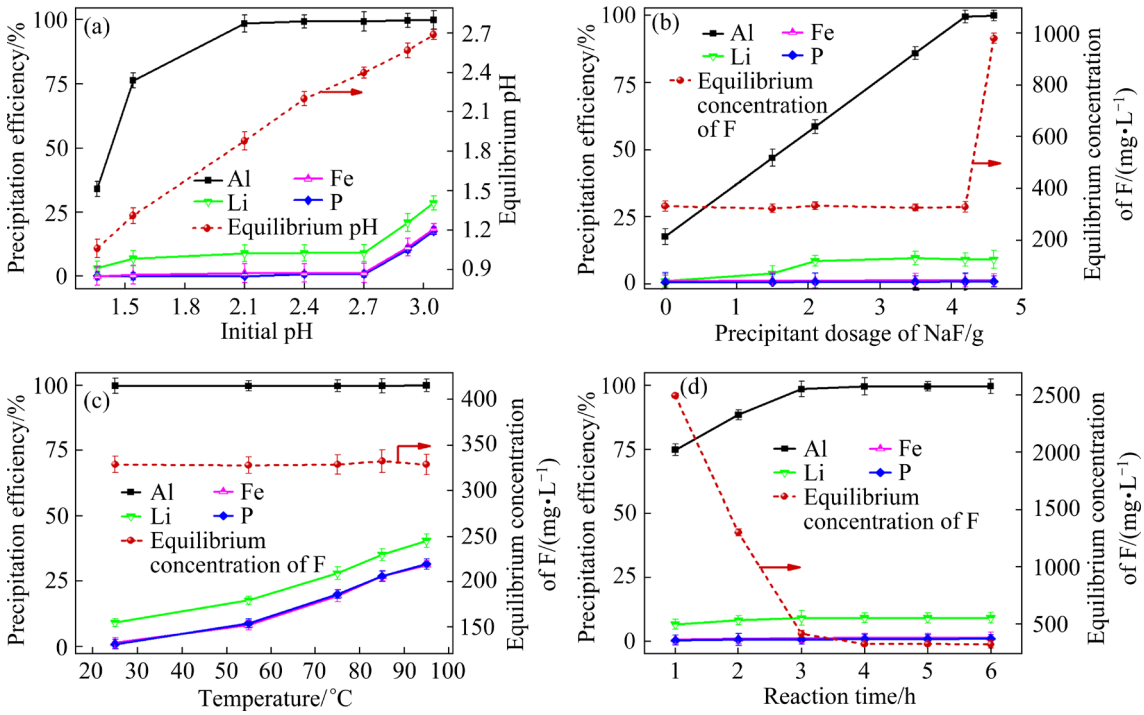

Fig. 4 Effects of different parameters for selective fluorinated coordination precipitation for Al: (a) Initial pH (NaF dosage 4.2 g, 25 °C, 5 h); (b) Precipitant dosage of NaF (pH 2.4, 25 °C, 5 h); (c) Temperature (NaF dosage 4.2 g, pH 2.4, 5 h); (d) Reaction time (NaF dosage 4.2 g, pH 2.4, 25 °C)

can significantly diminish the content of F in the solution, which is beneficial to reducing the subsequent environmental costs. Excessive addition of NaF had a negligible promotion for the precipitation of Al, but would increase the reagent costs. The addition amount of NaF was determined to be 4.2 g, and the equilibrium concentration of F was 328.3 mg/L.

Figures 4(c, d) show the effects of temperature and reaction time on the removal of Al from the leachate. The reaction temperature had no obvious effect on Al precipitation, while high temperature would lead to the loss of Li, Fe, and P due to the formation of $LiFePO_4$. Furthermore, the removal for Al impurity in the first 3 h was rapid with precipitation efficiency over 98.0%. Further extension of reaction time had a negligible effect. Therefore, the precipitation processes were carried out at 298 K for 5 h in the subsequent experiments.

Furthermore, three parallel scale-up tests were conducted using 2.5 L Al/F-bearing leachate under the optimized conditions, indicating that the precipitation efficiencies of Al and F were 99.4% and 96.4%, respectively (Table S4 in SI). And the concentration of Al in the filtrate was only 0.0124 g/L, laying a foundation for the regeneration of Fe/P in the form of $FePO_4·2H_2O$.

Meanwhile, the generated residue (the composition (wt.%): Al 12.1, Li 4.7, Na 15.5, Fe 5.1, and P 1.7) was characterized by XRD, FT-IR, XPS, and SEM−EDS to further investigate the precipitation mechanism. The diffraction peaks presented good crystallinity and matched nicely with the standard PDF card of $Na_3Li_3Al_2F_{12}$ (#75-1571) (Fig. 5(a)). The crystal structure of cryolithionite $Na_3Li_3Al_2F_{12}$ consists of $[AlF_6]$ octahedron connected with the $[LiF_4]$ tetrahedron by sharing the same vertex, and sharing an edge with the $[NaF_8]$ dodecahedron, forming a three-dimensional network with numerous voids and channels [30].

The peaks at 3448.40 and 1631.07 cm^{-1} corresponded to the stretching vibration and bending vibrations of O—H bands in the molecules [31], respectively (Fig. 5(b)). The telescopic vibration of P—O was observed at 1079.75 cm^{-1} [32], while the bending vibration around 588.75 cm^{-1} corresponded to the F—Al—F bond [33]. Based on electronegativity difference, the strong vibrations at 1351.02 and 1385.68cm^{-1} were ascribed to Na—F and Li—F, respectively.

As shown in Fig. 5, the presence of Li, Fe, P, O, C, and F with no impurity peaks was identified, which supported the XRD and FT-IR analyses. The C 1s at 284.8 eV was used as the binding energy reference. The F 1s spectrum was fitted into three peaks corresponding to Na—F (685.51 eV), Li—F (684.99 eV), and Al—F (683.94 eV) bonds, with peak area ratio of 4∶2∶3, which was consistent with the cryolithionite structure [34]. The Al 2p spectrum was deconvoluted into two peaks of Al—F and Al—O, while O 1s peaks at 524.78, 531.48, and 536.98 eV arose from oxygen atoms in various structural bonds: O — Al, O — H, and O — P, respectively [35]. The Na 1s (1071.18 eV) and Li 1s (56.48 eV) spectra were fitted to a single broad peak, suggesting that only one type of bonding was possible in the compound. The SEM images (Fig. S2 in SI) demonstrated that the Al, F, and Na elements were uniformly distributed.

3.3 Synthesis of iron phosphate

The standard Gibbs free energy changes ($\Delta G^{\ominus}$) for the precipitation of $FePO_4·2H_2O$ were calculated using the HSC 6.0 software, and the temperature dependence of $\Delta G^{\ominus}$ is shown in Fig. 6(a). It is evident that the $\Delta G^{\ominus}$ of iron phosphate synthesis becomes more negative with elevated temperature, illustrating that the precipitation process is thermodynamically favorable.

The effect of reaction temperature on the precipitation of Fe/P in the temperature range of 75−98 °C was evaluated, and the results are shown in Fig. 6(b). At 75 °C, the precipitation efficiencies of Fe and P were 82.9% and 79.5%, respectively, resulting in slightly lower than theoretical contents of Fe (27.4 wt.%) and P (15.9 wt.%) in products. Within the temperature range of 85−98 °C, the Fe/P molar ratio was maintained at 1∶1. Besides, the tap density of products initially decreased and then increased (Fig. 6(c)), while the characteristic XRD peak intensities of products initially increased and then decreased (Fig. 6(d)), attributing to the fact that low temperature prompted particle growth, and agglomeration occurred at high temperature.

The $FePO_4·2H_2O$ precipitates obtained at 90 °C were subjected to calcination at 550 °C for 3 h, resulting in the generation of $FePO_4$ product [36]. The quality of the synthesized $FePO_4$ and the

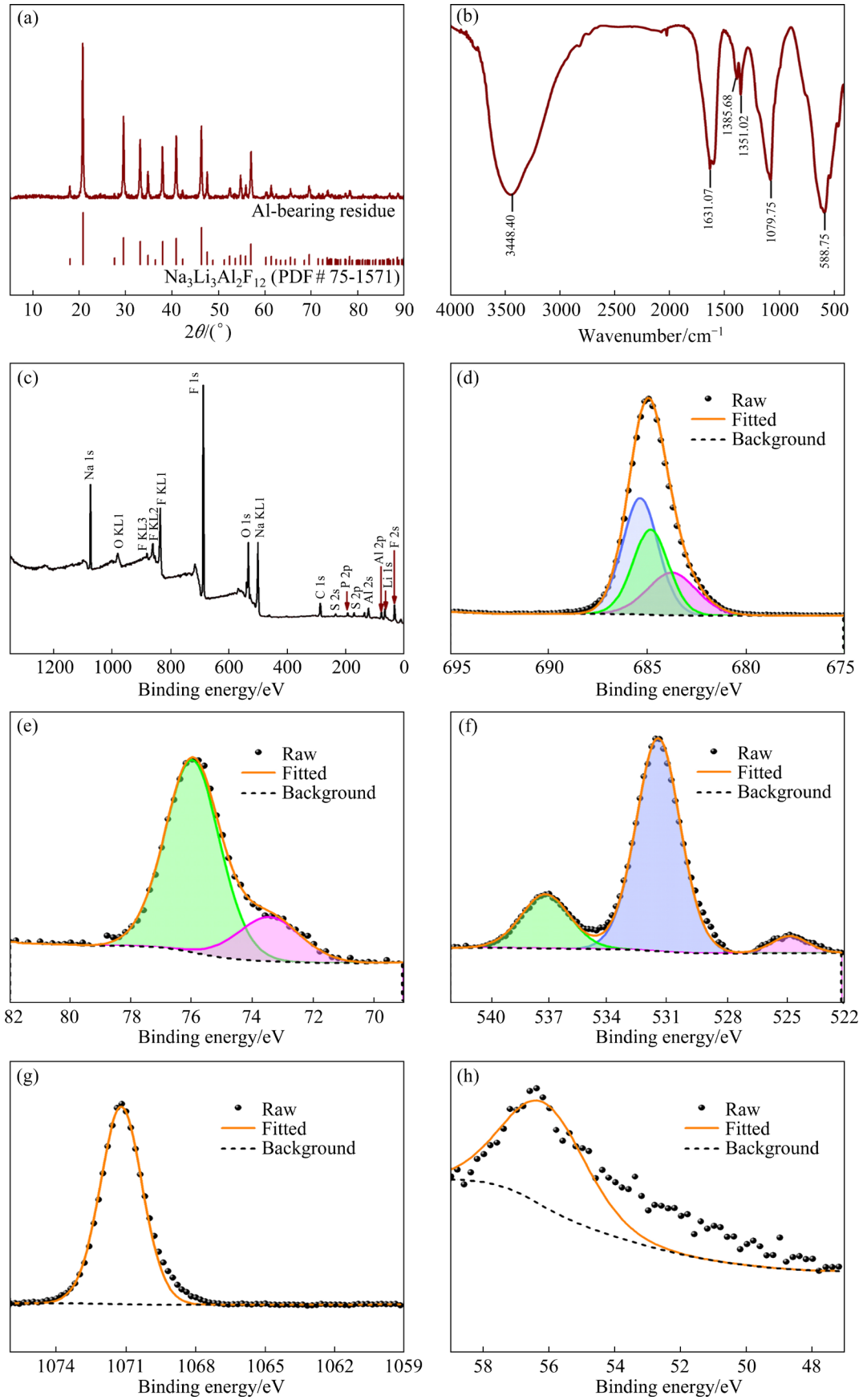

Fig. 5 (a) XRD patterns, (b) FT-IR spectra, (c) XPS spectra, and high-resolution XPS spectra for (d) F 1s, (e) Al 2p, (f) O 1s, (g) Na 1s, and (h) Li 1s of precipitate

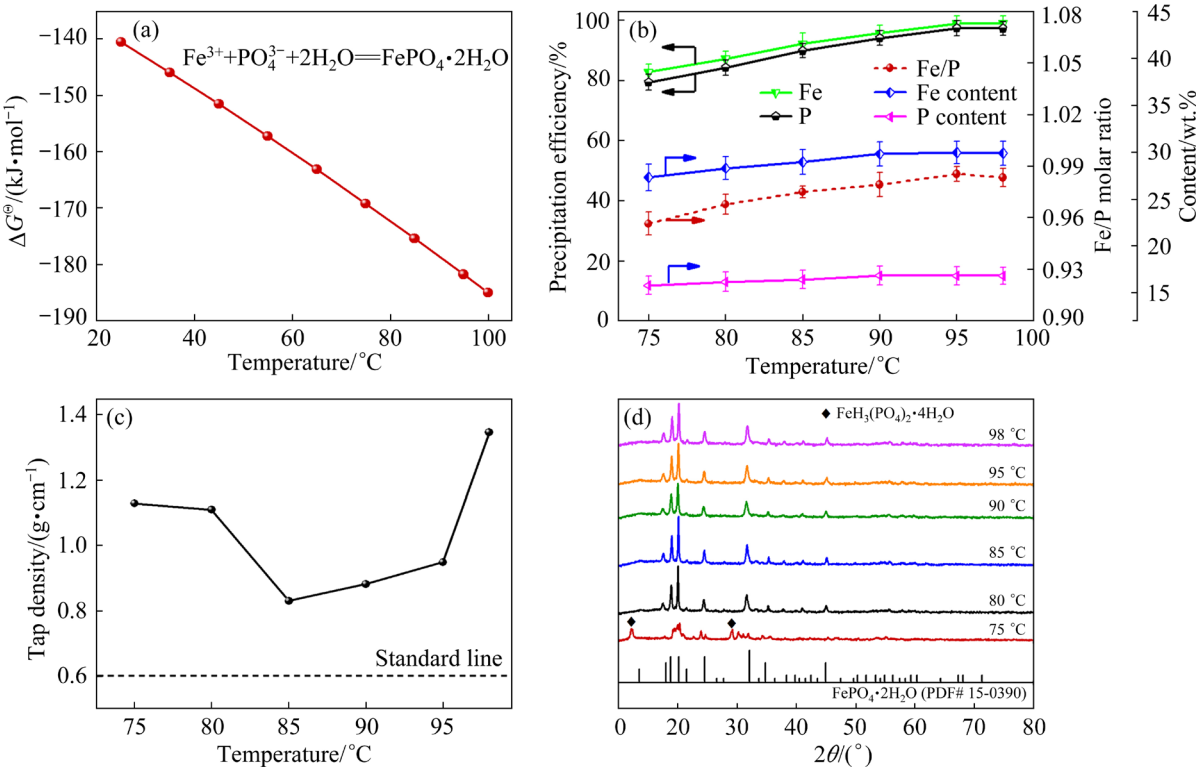

Fig. 6 (a) ΔG^{Θ} of precipitation reaction versus temperature, (b) effect of temperature on $FePO_4·2H_2O$ precipitation, (c) tap density and (d) XRD patterns of $FePO_4·2H_2O$ products at various temperatures

content of impurities presented in Table S5 of SI meet the battery grade purity standards in China (HG/T 4701—2021 Iron Phosphate for Battery Materials). XRD patterns in Fig. S3(a) of SI demonstrated that the synthesized $FePO_4$ closely matched the characteristic peaks of the $FePO_4$ standard (PDF# 84-0876). The synthesized $FePO_4$ displayed uniform distribution, with a median particle size (D_{50}) of 25.573 μm (Fig. S3(b) in SI).

Figure S3(c) in SI confirmed that the obtained $FePO_4$ product consisted of Fe, O, and P. The Fe 2p peaks were evident by their peculiar profile owing to multiple splitting (Fig. S3(d) in SI). The peaks with a binding energy of 725.55 and 712.37 eV were assigned to Fe $2P_{1/2}$ and Fe $2P_{3/2}$, respectively [37], and the peaks at 716.42, 719.96, and 729.08 eV were ascribed to the satellite peaks, designating the presence of Fe^{3+} in the products. The fitting peaks of O 1s spectrum (Fig. S3(e) in SI) consisted of two peaks, owing to orthogonal PO_4 tetrahedral and FeO_6 octahedral olivine structures, respectively [38]. The P 2p spectrum (Fig. S3(f) in SI) could be deconvoluted into two peaks centered at 133.35 and 134.32 eV, which were related to —P═O (P $2p_{3/2}$) and —P—O (P $2p_{1/2}$) groups in PO_4^{3-} polyanion, respectively [39].

The morphology images of $FePO_4$ product revealed the formation of near-spherical shaped precipitates with micro sheet aggregates on the surface, which were conductive to Li^+ migration (Figs. S4(a, b) in SI). Elemental analysis showed high purity of the product (Fig. S4(c) in SI). The AFM micrograph in Fig. S4(d) of SI demonstrated the dark zone surrounding the particle surface and the light top zone, with the value of root mean square roughness (R_q) of approximately 85.3 nm and the height of 276.3 nm (Fig. S4(e) in SI), comparable to the roughness in the SEM images.

3.4 Recovery of lithium carbonate

The lithium recovery from the fluorinated precipitation Al/F-bearing residue was achieved through a $CaCO_3$−$CaSO_4$ roasting (800 °C for 2 h) followed by acid leaching process. Acid leaching agent was derived from the synthetic filtrate of iron phosphate, supplemented with H_2SO_4. The main chemical reactions are outlined in Eqs. (1)−(3). Obviously, fluorine was fixed in the form of CaF_2 and LiF, so fluorine was not detected in the tail gas. Moreover, the thermodynamic calculations

indicated that the reactions of leaching process are thermodynamically feasible:

$$2Na_3Li_3Al_2F_{12}+6CaCO_3+4CaSO_4 = 10CaF_2+3Na_2SO_4+Li_2SO_4+2Al_2O_3+4LiF+6CO_2 \quad (1)$$

$$LiF+H_2SO_4 = Li^++SO_4^{2-}+HF, \quad \Delta G^{\Theta}\ (298.15\ K)=-31.125\ kJ/mol \quad (2)$$

$$LiF+HF = Li^++HF_2^-, \quad \Delta G^{\Theta}\ (298.15\ K)=-239.396\ kJ/mol \quad (3)$$

The phase evolution between the roasting product and leaching residue is shown in Fig. 7. The XRD analysis revealed that the roasting product was primarily composed of CaF_2, LiF, Al_2O_3, CaO, $CaSO_4$, and NaF. Notably, the LiF, CaO, and NaF phases almost disappeared from the leaching residue, and the fluorine remained in the form of CaF_2 in the residue.

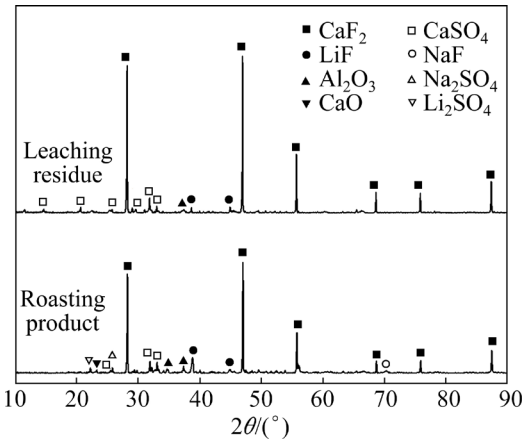

Fig. 7 XRD patterns of roasting product and leaching residue

The concentration of Li in the resulting solution was concentrated to about 20 g/L to enhance the recovery rate. And the composition of purified Li-rich solution is presented in Table S6 of SI, which could be directly used to synthesize lithium carbonate. The XRD pattern of the synthesized Li_2CO_3 product in Fig. 8(a) suggested that all diffraction peaks matched nicely with the standard PDF card (Li_2CO_3 #83-1454). The characteristic of the 4000−1500 cm^{-1} region in the FT-IR spectra (Fig. 8(b)) suggested the absence of —OH group, revealing the absence of water molecules in the products. The peaks at 1412.46, 1086.71, and 857.04 cm^{-1} for the product were ascribed to $\nu(CO_3^{2-})$, ν(C — O), and $\delta(CO_3^{2-})$, respectively, and the adsorption at 478.24 cm^{-1} was related to Li—O vibration [40].

Moreover, the purity of recovered Li_2CO_3 was confirmed by SEM−EDS, as shown in Figs. 9(a−c). The Li_2CO_3 crystals displayed as the massive agglomerates of bar-shaped distribution like cluster with no impurities detected. The purity of Li_2CO_3 could reach 99.87%, meeting the standards of High-purity Lithium Carbonate (YS/T 582—2013) (Table S7 in SI).

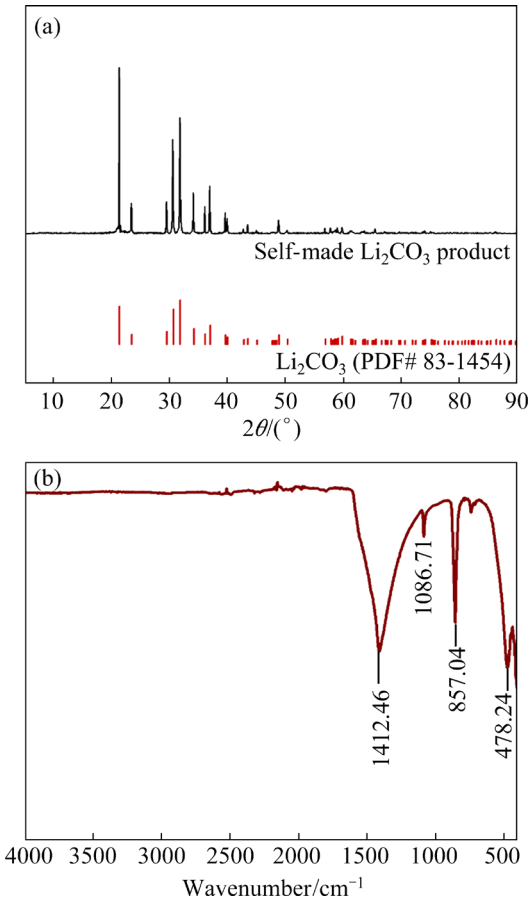

Fig. 8 (a) XRD pattern and (b) FT-IR spectrum of self-made Li_2CO_3 product

3.5 Integrated process for full resource recovery from spent LFPs

Based on the abovementioned results and analyses, a sustainable and high-value process for recycling $FePO_4$ and Li_2CO_3 products from Al/F-bearing spent LFPs was developed (Fig. 10). The process started with sulfuric acid leaching to extract valuable elements from the Al/F-bearing spent $LiFePO_4$/C powder, while Al removal was achieved through fluorinated coordination precipitation. The low-Al filtrate was then used to prepare the battery grade $FePO_4·2H_2O$ via

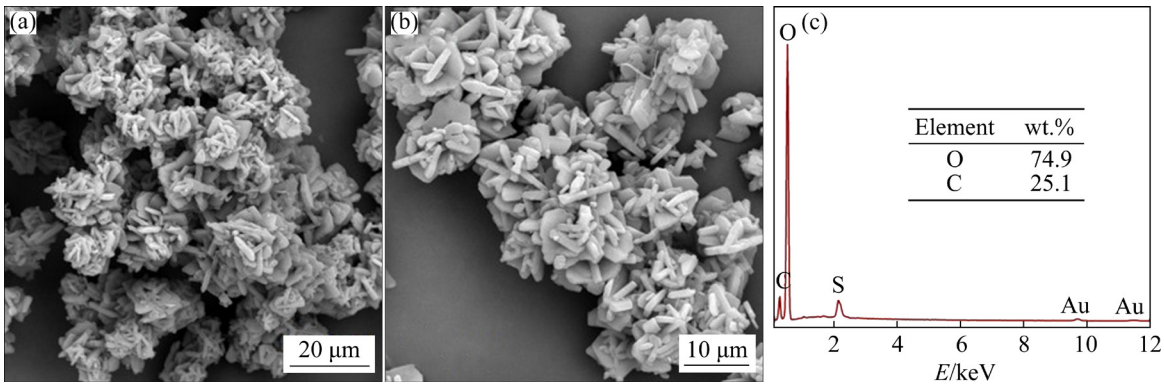

Fig. 9 (a, b) SEM images, and (c) EDS results of self-made Li_2CO_3 product

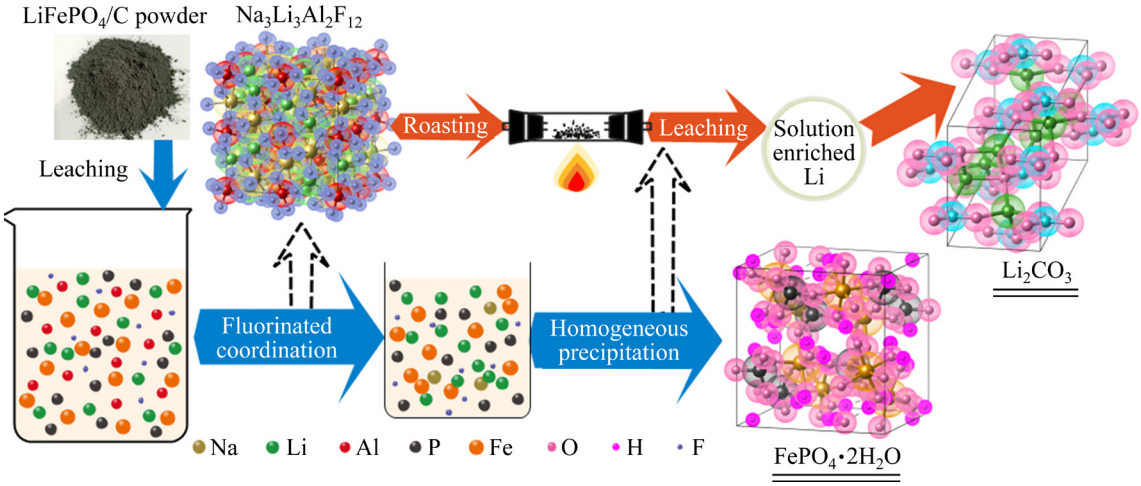

Fig. 10 Flow diagram of proposed method for treating Al/F-bearing spent $LiFePO_4$/C powder

homogeneous precipitation, and lithium in the precipitate of $Na_3Li_3Al_2F_{12}$ could be recycled through $CaCO_3$−$CaSO_4$ roasting followed by acid leaching, and fluorine was fixed in the form of CaF_2. The acidic filtrate generated in the synthesis of $FePO_4·2H_2O$ was used to leach the roasting residue, thus improving the concentration of Li in the solution. Finally, Li_2CO_3 product (99.87%) was prepared by the addition of Na_2CO_3, and the fluoride in the filtrate could be returned to the fluorinated coordination precipitation step. And the recovery rates of Li and Fe calculated with the mass balance diagram presented in Fig. S5 of SI were 96.88% and 92.85%, respectively.

Furthermore, A preliminary economic analysis was carried out for recycling 1 t of Al/F-bearing spent $LiFePO_4$/C powder by the proposed approach. The detailed calculation process and results are presented in Text S2 and Table S8 of SI. As shown in Fig. 11, the total costs were US$ 2427.31, and the reagents accounted for only 15.8% of all costs. The

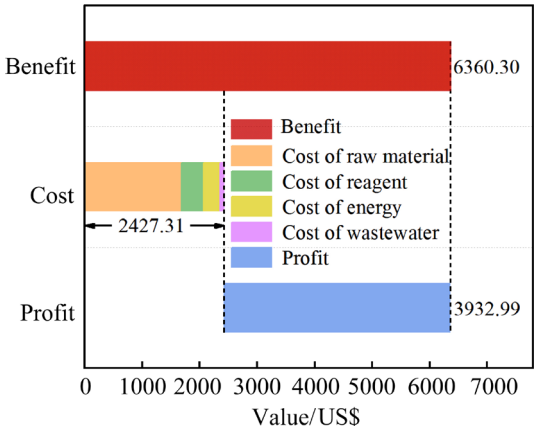

Fig. 11 Preliminary evaluation of total costs and benefits of recycling 1 t of Al/F-bearing spent $LiFePO_4$/C powder

calculated processing benefit was US$ 6360.30 per ton $LiFePO_4$/C powder and the corresponding profit was US$ 3932.99 per ton, considering the cost of electric energy and wastewater treatment. This demonstrated the economic feasibility of this method, which also had great advantages over the

existing alternative method presented in Table S9 of SI. Obviously, the purification process was simplified in a more effective manner, and additional profit could be obtained through the comprehensive recovery of Fe, P, and Li as battery grade $FePO_4$ and Li_2CO_3. This breakthrough filled a critical gap in the life cycle of $LiFePO_4$/C batteries.

4 Conclusions

(1) The regeneration of $FePO_4$ and Li_2CO_3 from Al/F-bearing spent $LiFePO_4$/C powder was successfully achieved by an integrated process involving sulfuric acid leaching, fluorinated coordination precipitation, homogeneous precipitation, and chemical precipitation.

(2) About 99.4% Al and 96.4% F in the Al/F-bearing solution were precipitated in the form of $Na_3Li_3Al_2F_{12}$, reducing the concentrations of Al and F in the solution to 0.0124 and 0.328 g/L, respectively. The obtained low-Al filtrate was directly used to prepare battery grade $FePO_4·2H_2O$ through homogeneous precipitation at high temperature, and the recovery rate of Fe was 92.85%.

(3) XRD results confirmed the formation of LiF by roasting $Na_3Li_3Al_2F_{12}$ with $CaCO_3$−$CaSO_4$, which could be dissolved by the acidic filtrate produced during the synthesis of $FePO_4·2H_2O$ supplemented with H_2SO_4. The obtained Li-rich solution could be further processed to obtain high-purity Li_2CO_3, and the recovery rate of Li was 96.88%.

(4) A preliminary economic cost analysis demonstrated the corresponding profit was US$ 3932.99 per ton, further illustrating that the proposed approach for the recovery of valuable components from Al/F-bearing spent $LiFePO_4$/C powder was efficient and sustainable.

CRediT authorship contribution statement

Ye-hui-zi WU: Investigation, Conceptualization, Methodology, Formal analysis, Data curation, Visualization, Writing − Original draft; **Kang-gen ZHOU:** Formal analysis, Methodology; **Chang-hong PENG:** Formal analysis, Methodology; **Kui YI:** Investigation, Validation; **Jing-kun DENG:** Validation, Data curation; **Zai-rong QIU:** Validation, Data curation; **Wei CHEN:** Conceptualization, Supervision, Writing − Review & editing, Project administration, Funding acquisition; **Ke-jing ZHANG:** Conceptualization, Supervision, Writing − Review & editing.

Declaration of competing interest

The authors declare that they have no known competing financial interests or personal relationships that could have appeared to influence the work reported in this paper.

Acknowledgments

This work was financially supported by the Key Research and Development Program of Guangxi, China (No. GUIKE AB23026051), the Science and Technology Innovation Program of Hunan Province, China (No. 2023RC3039), and the Fundamental Research Funds for the Central Universities of Central South University, China.

Supporting Information

Supporting Information in this paper can be found at: http://tnmsc.csu.edu.cn/download/24-p3520-2024-0016-Supporting-Information.pdf.

References

[1] WANG Ya-hui, WU Ji-jun, HU Guo-chen, MA Wen-hui. Recovery of Li and Fe from spent lithium iron phosphate using organic acid leaching system [J]. Transactions of Nonferrous Metals Society of China, 2024, 34(1): 336−346.

[2] QU Li-li, HE Ya-qun, FU Yuan-peng, XIE Wei-ning, YE Cui-ling, LU Qi-chang, LI Jin-long, LI Jia-hao, PANG Zhi-bo. Enhancement of leaching of cobalt and lithium from spent lithium-ion batteries by mechanochemical process [J]. Transactions of Nonferrous Metals Society of China, 2022, 32(4): 1325−1335.

[3] WANG Zi-xuan, WU Dan-dan, WANG Xi, HUANG Ye, WU Xu. Green phosphate route of regeneration of $LiFePO_4$ composite materials from spent lithium-ion batteries [J]. Industrial & Engineering Chemistry Research, 2023, 62(2): 1181−1194.

[4] TIAN Lun, YANG Yu-shun, CHEN Gui-jing, TIRAFERRI A, LIU Bai-cang. Efficient lithium extraction from shale gas wastewater using sodium alginate/$H_{1.33}Mn_{1.67}O_4$ composite granular adsorbents [J]. ACS ES&T Engineering, 2023, 3(11): 1676−1685.

[5] WU Li-xiang, ZHANG Fu-shen, ZHANG Zhi-yuan, ZHANG Cong-cong. An environmentally friendly process for selective recovery of lithium and simultaneous synthesis of $LiFe_5O_8$ from spent $LiFePO_4$ battery by mechanochemical [J]. Journal of Cleaner Production, 2023, 396: 136504.

[6] REN Guo-xing, LIAO Cai-bin, LIU Zhi-hong, XIAO Song-wen. Lithium and manganese extraction from manganese-rich slag originated from pyrometallurgy of spent lithium-ion battery [J]. Transactions of Nonferrous Metals Society of China, 2022, 32(8): 2746−2756.

[7] YANG Li-ming, GAO Zhe, LIU Tian, HUANG Mei-ting, LIU Guang-zhen, FENG Yu-fa, SHAO Peng-hui, LUO Xu-biao. Direct electrochemical leaching method for high-purity lithium recovery from spent lithium batteries [J]. Environmental Science & Technology, 2023, 57(11): 4591−4597.

[8] ZHOU Hui-xiang, LUO Zhong-yan, WANG Shuai, MA Xin, CAO Zhan-fang. A mild closed-loop process for lithium–iron separation and cathode materials regeneration from spent $LiFePO_4$ batteries [J]. Separation and Purification Technology, 2023, 315: 123742.

[9] YANG Jian, ZHOU Yuan, ZHANG Zong-liang, XU Kai-hua, ZHANG Kun, LAI Yan-qing, JIANG Liang-xing. Effect of electric field on leaching valuable metals from spent lithium-ion batteries [J]. Transactions of Nonferrous Metals Society of China, 2023, 33(2): 632−641.

[10] SUN Jing, JIANG Zhen-yu, JIA Ping-shan, LI Su, WANG Wen-long, SONG Zhan-long, MAO Yan-peng, ZHAO Xi-qiang, ZHOU Bing-qian. A sustainable revival process for defective $LiFePO_4$ cathodes through the synergy of defect-targeted healing and in-situ construction of 3D-interconnected porous carbon networks [J]. Waste Management, 2023, 158: 125−135.

[11] XU Yun-long, QIU Xue-jing, ZHANG Bai-chao, Di An-di, DENG Wen-tao, ZOU Guo-qiang, HOU Hong-shuai, JI Xiao-bo. Start from the source: Direct treatment of a degraded $LiFePO_4$ cathode for efficient recycling of spent lithium-ion batteries [J]. Green Chemistry, 2022, 24(19): 7448−7457.

[12] WANG Wei, WU Yu-feng. An overview of recycling and treatment of spent $LiFePO_4$ batteries in China [J]. Resources, Conservation and Recycling, 2017, 127: 233−243.

[13] WU De-you, WANG Dong-xing, LIU Zhi-qiang, RAO Shuai, ZHANG Kui-fang. Selective recovery of lithium from spent lithium iron phosphate batteries using oxidation pressure sulfuric acid leaching system [J]. Transactions of Nonferrous Metals Society of China, 2022, 32(6): 2071−2079.

[14] ZHANG Liang-jun, TENG Tao, XIAO Li, SHEN Li, RAN Jian-jun, ZHENG Jiang-feng, ZHU Yi-rong, CHEN Han. Recovery of $LiFePO_4$ from used lithium-ion batteries by sodium-bisulphate-assisted roasting [J]. Journal of Cleaner Production, 2022, 379: 134748.

[15] ZHONG Xiao-cong, CHEN Chen, YAN Kang, ZHANG Kui-fang, WANG Rui-Xiang, XU Zhi-feng. Influence of sulfate ion on fluoride removal from flue gas scrubbing wastewater using lanthanum salts [J]. Transactions of Nonferrous Metals Society of China, 2023, 33(11): 3560−3569.

[16] WU Ye-hui-zi, ZHOU Kang-gen, ZHANG Xue-kai, CHEN Wei, DENG Jing-kun, HE De-wen, PENG Chang-hong. Al/Ti removal from the sulfate leachate of the spent $LiFePO_4$/C powder through high-temperature co-precipitation triggered by Fe(III) [J]. Industrial & Engineering Chemistry Research, 2023, 62(35): 13902−13910.

[17] XIE Hui, ZHOU Zhen-tao. Physical and electrochemical properties of mix-doped lithium iron phosphate as cathode material for lithium-ion battery [J]. Electrochimica Acta, 2006, 51(10): 2063−2067.

[18] XU Jing, CHEN Gang, TENG Yu-Jie, ZHANG Bin. Electrochemical properties of $LiAl_xFe_{1-3x/2}PO_4$/C prepared by a solution method [J]. Solid State Communications, 2008, 147(9/10): 414−418.

[19] YANG Mu-rong, KE Wei-hsin. The doping effect on the electrochemical properties of $LiFe_{0.95}M_{0.05}PO_4$ (M=Mg^{2+}, Ni^{2+}, Al^{3+}, or V^{3+}) as cathode materials for lithium-ion cells [J]. Journal of the Electrochemical Society, 2008, 155(10): A729.

[20] LOU Wen-bo, ZHANG Yang, ZHANG Ying, ZHENG Shi-li, SUN Pei, WANG Xiao-jian, LI Jian-zhong, QIAO Shan, ZHANG Yi, WENZEIL M, WEIGAND J J. Leaching performance of Al-bearing spent $LiFePO_4$ cathode powder in H_2SO_4 aqueous solution [J]. Transactions of Nonferrous Metals Society of China, 2021, 31(3): 817−831.

[21] LI Zheng, HE Li-hua, ZHU Yun-fei, YANG Chao. A green and cost-effective method for production of LiOH from spent $LiFePO_4$ [J]. ACS Sustainable Chemistry & Engineering, 2020, 8(42): 15915−15926.

[22] JI Guan-jun, WANG Jun-xiong, LIANG Zheng, JIA Kai, MA Jun, ZHUANG Zhao-feng, ZHOU Guang-min, CHENG Hui-ming. Direct regeneration of degraded lithium-ion battery cathodes with a multifunctional organic lithium salt [J]. Nature Communications, 2023, 14(1): 584.

[23] WANG Xiao-ming, PHILLIPS B, BOILY J F, HU Yong-feng, HU Zhen, YANG Peng, FENG Xiong-han, XU Wen-qian, ZHU Meng-qiang. 2019. Phosphate sorption speciation and precipitation mechanisms on amorphous aluminum hydroxide [J]. Soil Systems, 2019, 3(1): 20.

[24] LI Li, BIAN Yi-fan, ZHANG Xiao-xiao, YAO Ying, XUE Qing, FAN Er-sha, WU Feng, CHEN Ren-jie. A green and effective room-temperature recycling process of $LiFePO_4$ cathode materials for lithium-ion batteries [J]. Waste Management, 2019, 85: 437−444.

[25] DAI Yang, XU Zhao-dong, HUA Dong, GU Han-nian, WANG Ning. Theoretical-molar Fe^{3+} recovering lithium from spent $LiFePO_4$ batteries: An acid-free, efficient, and selective process [J]. Journal of Hazardous Materials, 2020, 396: 122707.

[26] XU Zhao-dong, DAI Yang, HUA Dong, GU Han-nian, WANG Ning. Creative method for efficiently leaching Ni, Co, Mn, and Li in a mixture of $LiFePO_4$ and $LiMO_2$ using only Fe(III) [J]. ACS Sustainable Chemistry & Engineering, 2021, 9(11): 3979−3984.

[27] WU Ye-hui-zi, ZHOU Kang-gen, ZHANG Xue-kai, PENG Chang-hong, JIANG Yang, CHEN Wei. Aluminum separation by sulfuric acid leaching-solvent extraction from Al-bearing $LiFePO_4$/C powder for recycling of Fe/P [J]. Waste Management, 2022, 144: 303−312.

[28] CHEN Bing-xu, PENG Jian-ping, WANG Yao-wu, DI Yue-zhong. Penetration behavior of electrolyte into graphite cathode in NaF−KF−LiF−AlF_3 system with low cryolite ratios [J]. Transactions of Nonferrous Metals Society of China, 2022, 32(8): 2727−2735.

[29] JING Qian-kun, ZHANG Jia-liang, LIU Yu-bo, YANG Cheng, MA Bao-zhong, CHEN Yong-qiang, WANG Cheng-yan. E-pH Diagrams for the Li−Fe−P−H_2O system from 298 to 473 K: Thermodynamic analysis and application to the wet chemical processes of the $LiFePO_4$ cathode

material [J]. The Journal of Physical Chemistry C, 2019, 123(23): 14207−14215.

[30] LI Hong, LIU Yan, TANG Shu, LUO Li-jun, ZHOU Qiang, WANG Zheng-liang. Luminescence properties of Mn^{4+} with high ^2Eg level energy in the polyfluoride $Na_3Li_3Sc_2F_{12}$ [J]. Dalton Transactions, 2020, 49(33): 11613−11617.

[31] GUO Hui, YU Hai-zhao, ZHOU An-an, LU Meng-hua, WANG Qiao, KUANG Ge, WANG Hai-dong. Kinetics of leaching lithium from α-spodumene in enhanced acid treatment using HF/H_2SO_4 as medium [J]. Transactions of Nonferrous Metals Society of China, 2019, 29(2): 407−415.

[32] ZHENG Ru-juan, ZHAO Li, WANG Wen-hui, LIU Yuan-long, MA Quan-xin, MU De-ying-, LI Ru-hong, DAI Chang-song. Optimized Li and Fe recovery from spent lithium-ion batteries via a solution-precipitation method [J]. RSC Advances, 2016, 6(49): 43613−43625.

[33] DUBEY S, AGARWAL M, GUPTA A B. Experimental investigation of Al−F species formation and transformation during coagulation for fluoride removal using alum and PACl [J]. Journal of Molecular Liquids, 2018, 266: 349−360.

[34] MUNIRATHNAM K, DILLIP G R, CHAURASIA S, JOO S W, DEVA P R B, JOHN S N. Investigations on surface chemical analysis using X-ray photoelectron spectroscopy and optical properties of Dy^{3+}-doped $LiNa_3P_2O_7$ phosphor [J]. Journal of Molecular Structure, 2016, 1118: 117−123.

[35] ZHAO Na-na, ZHANG Feng-chu, ZHAN Fei, YI Ding, YANG Yi-jun, CUI Wei-bin, WANG Xi. Fe^{3+}-stabilized Ti_3C_2T MXene enables ultrastable Li-ion storage at low temperature [J]. Journal of Materials Science & Technology, 2021, 67: 156−164.

[36] ZHANG Xue-kai, ZHOU Kang-gen, ZENG De-wen, Li Jia, WU Ye-hui-zi, CHEN Wei, PENG Chang-hong Peng. Preparation of battery-grade $FePO_4·2H_2O$ using the stripping solution generated from resource recycling of bauxite residue [J]. Bulletin of Environmental Contamination and Toxicology, 2022, 109(1): 86−94.

[37] MAHANDRA H, HEIN G, FARAJI F, GHAHREMAN Ahmad. A novel neutrophilic bacteria-based process for selective $LiFePO_4$ cathode recycling [J]. Resources, Conservation and Recycling, 2023, 195: 107015.

[38] HU Guo-rong, GONG Yi-fan, PENG Zhong-dong, DU Ke, HUANG Min, WU Jia-hui, GUAN Di-chang, ZENG Jing-yao, ZHANG Bai-chao Zhang, CAO Yan-bing. Direct recycling strategy for spent lithium iron phosphate powder: An efficient and wastewater-free process [J]. ACS Sustainable Chemistry & Engineering, 2022, 10(35): 11606−11616.

[39] LI Yong-qiang, ZHOU Yue, MA Wen-long, WU Ping, CAO Xin, ZHU Xiao-shu, WEI Shao-hua, ZHOU Yi-ming. Facile fabrication of the hybrid of amorphous $FePO_4·2H_2O$ and GO toward high-performance sodium-ion batteries [J]. Journal of Physics and Chemistry of Solids, 2023, 176: 111243.

[40] LI Shu-dan, LI Ting, WANG Chen-yi, GAO Kun. A comparative study of Li_2CO_3 modified carbon microbead anodes prepared by different synthetic routes for lithium-ion battery [J]. Ionics, 2016, 22(12): 2331−2339.

从含铝/氟的废 $LiFePO_4$/C 粉中再生电池级磷酸铁和碳酸锂

吴业惠子，周康根，彭长宏，易 葵，邓景焜，邱在容，陈 伟，张可菁

中南大学 冶金与环境学院，长沙 410083

摘 要：提出了一种可持续地从含铝/氟的废 $LiFePO_4$/C 粉中回收电池级磷酸铁和碳酸锂的方法，主要包括酸浸、氟化配位沉淀、均相沉淀和高温沉淀。在优化条件下，锂、铁、磷、铝和氟的浸出率分别为 97.6%、97.1%、97.1%、72.5%和 63.3%。系统研究了不同影响因素对脱除 Al/F 杂质的影响。结果显示，浸出液中 99.4%的铝和 96.4%的氟以 $Na_3Li_3Al_2F_{12}$ 的形式析出，滤液中两者的浓度分别为 0.0124 g/L 和 0.328 g/L，所得低铝滤液可直接制备出纯度为 99.68%的电池级磷酸铁。铝/氟沉淀渣中的锂可通过 $CaCO_3$−$CaSO_4$ 焙烧结合酸浸工艺有效提取，最终获得了纯度为 99.87%的 Li_2CO_3。锂和铁的回收率分别为 96.88%和 92.85%。经济效益评估表明该工艺是可盈利的。

关键词：含铝/氟的废 $LiFePO_4$/C 粉；硫酸浸出；杂质脱除；电池级磷酸铁；电池级碳酸锂

(Edited by Bing YANG)